Available online at www.sciencedirect.com
SCIENCE DIRECT®
Journal of Solid State Chemistry 179 (2006) 579–589
JOURNAL OF SOLID STATE CHEMISTRY
www.elsevier.com/locate/jssc

Synthesis, structural determination and magnetic properties of layered hybrid organic–inorganic, iron (II) propylphosphonate, $Fe[(CH_3(CH_2)_2PO_3)(H_2O)]$, and iron (II) octadecylphosphonate, $Fe[(CH_3(CH_2)_{17}PO_3)(H_2O)]$

Carlo Bellitto[a,1], Elvira M. Bauer[a], Philippe Léone[b,*], Alain Meerschaut[b], Catherine Guillot-Deudon[b], Guido Righini[a]

[a]*CNR-Istituto di Struttura della Materia, Sez.2, Via Salaria Km. 29.5, C.P.10, I-00016, Monterotondo Stazione, Roma, Italy*
[b]*CNRS-Université de Nantes, UMR 6502, Institut des Matériaux Jean Rouxel, 2 Rue de la, Houssinière, BP 32229, 44322 Nantes Cedex 03, France*

Received 16 September 2005; received in revised form 8 November 2005; accepted 12 November 2005
Available online 20 December 2005

Abstract

$Fe[(CH_3(CH_2)_2PO_3)(H_2O)]$ (**1**) and $Fe[(CH_3(CH_2)_{17}PO_3)(H_2O)]$ (**2**) were synthesized by reaction of $FeCl_2 \cdot 6H_2O$ and the relevant phosphonic acid in water in presence of urea and under inert atmosphere. The compounds were characterized by elemental and thermogravimetric analyses, UV–visible and IR spectroscopy. The crystal structure of (**1**) was determined from X-ray single crystal diffraction studies at room temperature: monoclinic symmetry, space group $P2_1$, $a = 5.707(1)$ Å, $b = 4.811(1)$ Å, $c = 11.818(2)$ Å, and $\beta = 98.62(3)^\circ$. The compound is lamellar and the structure is hybrid, made of alternating inorganic and organic layers along the c direction. The inorganic layers consist of Fe(II) ions octahedrally coordinated by five phosphonate oxygen atoms and one from the water molecule, separated by *bi*-layers of propyl groups. A preliminary structure characterization of compound (**2**) suggests a similar layered structure, but with an interlayer spacing of 40.3 Å. The magnetic properties of the compounds were both studied by a dc and ac SQUID magnetometer. $Fe[(CH_3(CH_2)_2PO_3)(H_2O)]$ (**1**) obeys the Curie–Weiss law at temperatures above 50 K ($C = 3.81\,cm^3\,K\,mol^{-1}$, $\theta = -62$ K), indicating a Fe +II oxidation state, a high-spin d^6 ($S = 2$) electronic configuration and an antiferromagnetic exchange couplings between the near-neighbouring Fe(II) ions. Below $T = 22$ K, $Fe[(CH_3(CH_2)_2PO_3)(H_2O)]$ exhibits a weak ferromagnetism. The critical temperature of $T_N = 22$ K has been determined by ac magnetic susceptibility measurements. Compound (**2**) shows the same paramagnetic behaviour of the iron (II) propyl derivative. The values of C and θ were found to be $3.8\,cm^3\,K\,mol^{-1}$ and -44 K, respectively, thus suggesting the presence of Fe +II ion in the $S = 2$ spin state and antiferromagnetic interactions between Fe(II) ions at low temperatures. Zero-field and field cooled magnetic susceptibility vs. T plots do not overlap below $T = 30$ K, suggesting the presence of an ordered magnetic state. The critical temperature, T_N, has been located by the peaks at $T_N = 26$ K from the *ac* susceptibility ($\chi'$and χ'') vs. T plots. Below T_N hysteresis loops recorded in the temperature region $16 < T < 26$ K show an S-shape, while below 15 K assume an ellipsoid form. They reveal that compound (**2**) is a weak ferromagnet. The critical temperature T_N in these layered Fe(II) alkylphosphonates is independent of the distance between the inorganic layers.

Keywords: Layered compounds; Magnetic properties; Iron phosphonates; Crystal structure

1. Introduction

Metal (II)-phosphonates $M[(RPO_3)(H_2O)]$, and *bis*-phosphonates $M_2[(O_3PRPO_3)(H_2O)_2]$ (where M is a divalent metal ion, and R is an alkyl or aryl group) represent an interesting class of hybrid organic–inorganic compounds [1]. M(II)$[(RPO_3)(H_2O)]$ (M = Cd, Mg, Mn,

*Corresponding author. Fax: +33 2 40373995.
E-mail addresses: Carlo.Bellitto@ism.cnr.it (C. Bellitto), Philippe.Leone@cnrs-imn.fr (P. Léone).
[1]Also correspondence to.

0022-4596/$ - see front matter © 2005 Elsevier Inc. All rights reserved.
doi:10.1016/j.jssc.2005.11.016

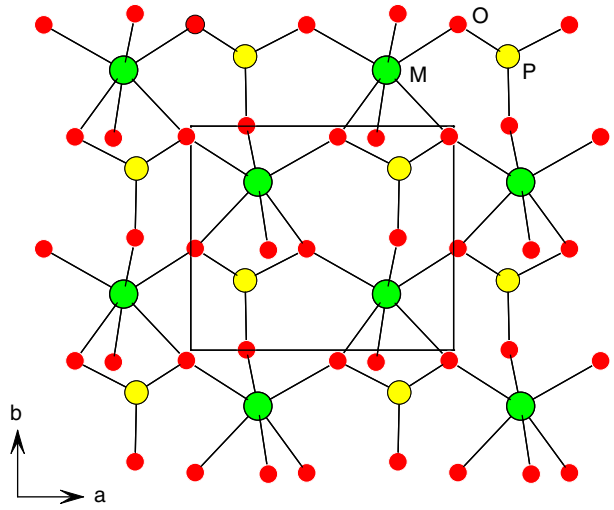

Fig. 1. Inorganic layer structure of divalent metal phosphonate.

Co, Zn) crystallize mainly in layered structures composed of metal ions and the phosphonate oxygen atoms lying in puckered sheets [2,3]. The pendent organic *R*-group occupies the interlamellar space and two organic layers having van der Waals contacts are interspersed to the inorganic ones. The number of carbon atoms in the organic chain can be varied and the interlayer distance can be then increased. It has been shown that the structures of divalent metal phosphonates tend to comprise zig-zag layers with the metal ion six-coordinated (see Fig. 1). For each phosphonate group two oxygen atoms form a bridge between a pair of metal atoms whereas the third oxygen is coordinated to only one metal atom. Each metal atom is thus coordinated by six oxygens in a distorted octahedral symmetry. These six oxygens comprise four bridging, one terminal and one from a water molecule. The resulting 2D lattice is interesting from the point of view of the search for new low-dimensional magnetic materials and for thin-film magnets. The two-dimensional nature of the crystal lattice in paramagnetic metal(II) phosphonates favours the next-neighbour exchange magnetic interaction and, at low temperatures, a long-range magnetic ordering is often observed [4].

We have recently reported on several paramagnetic divalent metal phosphonates such as $Cr[(CH_3PO_3)(H_2O)]$ [5], $Fe[CH_3CH_2PO_3)(H_2O)]$ [6], $Fe[C_6H_5PO_3)(H_2O)]$ [7], $Fe_2[(O_3P(CH_2)_2PO_3)\cdot(H_2O)_2]$ [8], $Fe[(CH_3PO_3)(H_2O)]$ [9,10] (CCDC 270703), and $Ni[(CH_3(CH_2)_{17}PO_3)(H_2O)]$ [11]. They were all found to be layered hybrid organic–inorganic compounds, which order antiferromagnetically at low temperatures. Below the magnetic ordering temperature (T_N), the magnetic moments are not perfectly antiparallel as it should be expected for an antiferromagnet, but canted thus giving rise to a spontaneous magnetization. This phenomenon is better known as "*canted antiferromagnetism*" or "*weak-ferromagnetism*" [12]. Moreover, by introducing another functional group into the ligand, an interesting polar compound of formula $Cr[(H_3N(CH_2)_2PO_3)(Cl)(H_2O)]$ [13] was isolated. The structure of the latter is again hybrid and consists of organic–inorganic layers held together by an alternation of ionic and covalent bonds. For divalent transition metals, most studies were carried out within the field of inorganic solid state chemistry and the main difficulty was the lack of a general procedure for the formation of the crystalline materials, possibly as single crystals. We have found a general method of preparation of metal(II) phosphonates, which provides at least a microcrystalline product, and in some cases has allowed to grow single crystals [9,10].

This paper deals with the synthesis and magnetic properties of two new iron (II) alkylphosphonates: $Fe[(CH_3(CH_2)_2PO_3)(H_2O)]$ (**1**) and $Fe[(CH_3(CH_2)_{17}PO_3)(H_2O)]$ (**2**), and the X-ray single crystal structure determination of $Fe[(CH_3(CH_2)_2PO_3)(H_2O)]$ (**1**). Both compounds were designed, prepared and studied with the aim of studying the influence of the organic thickness between the inorganic layers on their magnetic properties.

2. Experimental section

2.1. Materials and methods

Propylphosphonic acid, $CH_3(CH_2)_2PO_3H_2$, was of analytical grade (Aldrich Chemical Co.) and was used without further purification. Urea was of analytical grade (Carlo ERBA). The octadecylphosphonic acid, $CH_3(CH_2)_{17}PO_3H_2$ was prepared according to literature methods [14]. The compound was re-crystallized from ethanol and the purity checked by elemental analysis. HPLC water was used as solvent. All the reactions involving the Fe(II) ions were carried out under inert atmosphere by using Schlenck techniques.

2.2. Synthesis of $Fe[(CH_3(CH_2)_2PO_3)(H_2O)]$ (*1*)

We have prepared iron (II) organophosphonates from solution. For this purpose $FeSO_4\cdot 7H_2O$ (1.33 g, 4.78 mmol), $H_2O_3P(CH_2)_2CH_3$ (0.59 g, 4.78 mmol) and NH_2CONH_2 (0.51 g, 8.49 mmol, Acros p.a.) were placed in a pyrex heavy-walled ampoule of 50 mL size. The ampoule was put under vacuum by a vacuum line and purged with N_2 gas. To the ampoule was added degassed H_2O (20 mL) (Millipore) by a syringe and the ampoule sealed off under vacuum. The ampoule was then placed in a stainless tube, transferred to an oven and heated up to 90 °C for a few days. After a slow cooling a white microcrystalline powder was collected and washed several times with water (yield ~80%). The final pH of the filtrate was around 7.1. *Elemental analysis (weight %): C, 18.20; H, 4.35 (calculated : C, 18.39; H, 4.63).*

2.3. Synthesis $Fe[(CH_3(CH_2)_{17}PO_3)(H_2O)]$ (*2*)

The compound was prepared by following the above-described procedure. A mixture of $FeSO_4\cdot 7H_2O$ (1.33 g,

4.78 mmol), $CH_3(CH_2)_{17}PO_3H_2$ (1.59 g, 4.75 mmol) and NH_2CONH_2 (0.57 g, 9.49 mmol) was placed in an ampoule and purged with N_2 gas prior addition of a degassed solvent mixture (ethanol 5 mL/H_2O 10 mL). A white microcrystalline solid was isolated after a heat treatment at 80 °C for a few days (yield ~90%). The final pH of the filtrate was 7.1. *Elemental analysis (weight %): C, 53.10 ; H, 9.99 (calculated: C, 53.20; H, 9.67).*

2.4. Characterization and physical measurements

Elemental analyses were performed by the Servizio di Microanalisi della Area di Ricerca di Roma del CNR. Thermogravimetric (TGA) data were obtained in flowing dry nitrogen at a heating rate of 10°/min on a Stanton-Redcroft STA-781 thermoanalyzer. The FT-IR absorption spectra were recorded on a Perkin-Elmer 621 spectrophotometer using KBr pellets. Static magnetic susceptibility measurements were performed by using a Quantum Design MPMS-5S SQUID magnetometer in fields up to 5 T in the temperature range 2–300 K. The ac susceptibility was determined without dc magnetic field but with an ac field of 3 Oe and a frequency of 2, 20, and 200 Hz. A cellulose capsule was filled with a freshly prepared polycrystalline sample and placed inside a polyethylene straw at the end of the sample rod. All the experimental data were corrected for the core magnetization using Pascal's constants.

2.5. Crystallographic data collection and structure determination

Room temperature X-ray powder diffraction data were recorded on a Seifert XRD-3000 diffractometer, Bragg–Brentano geometry, equipped with a curved graphite monochromator [λ(Cu-$K_{\alpha1,2}$) = 1.54056/1.5444 Å] and a scintillator detector. The data were collected with a step size of 0.02° ($\Delta 2\theta$), and at count time of 8 s per step of 0.2° min^{-1} over the range $4° < 2\theta < 80°$. The sample was mounted on a flat glass plate giving rise to a strong preferred orientation. The diffractometer zero point was determined from an external Si standard.

2.5.1. Single crystal data collection and structure determination of $Fe[(CH_3(CH_2)_2PO_3)(H_2O)]$

Numerous crystals were tested for quality (intensity and shape of the spots) with a Nonius Kappa CCD diffractometer using Mo-$K\alpha$ radiation ($\lambda = 0.71073$ Å). After several attempts, a colourless platelet-shaped crystal of dimensions $0.5 \times 0.2 \times 0.02\ mm^3$, was isolated and used for data collection at room temperature. The symmetry was monoclinic with the following unit cell parameters: $a = 5.7070(11)$Å, $b = 4.8108(10)$Å, $c = 11.818(2)$Å, and $\beta = 98.62(3)°$. Operating conditions and X-ray crystallographic details are given in Table 1.

Analysis of the diffraction data (7014 reflections) by using the program XPREP [15] revealed two possible space groups: $P2_1$ and $P2_1/m$. The intensity statistics as well as the values of the figures of merit orientated our choice for the non-centrosymmetric space group $P2_1$. Lorentz, polarisation as well as absorption correction using the face indexing option (crystal delimited by faces {100} = 0.25 mm, {010} = 0.1 mm and {001} = 0.01 mm) were applied. The structure was solved by means of the direct methods (SHELXS program) and all subsequent calculations were carried out with the SHELXTL program [16]. The hydrogen positions of the propyl group were found from the DFIX and DANG instructions which restrain distances to target values, 0.96 and 1.57 Å for C–H and H–H, respectively. The hydrogen positions of the water molecule have also been found through the DFIX and DANG instructions with values of 0.92 and 1.5 Å for O–H and H–H, respectively. Fe and P atoms have been anisotropically refined. The final refinement converged to the *R*-values: $R_{obs} = 13.49\%$ for 1344 reflections ($I > 2\sigma(I)$) and $R_{all} = 13.91\%$ for all the 1450 reflections, with 74 parameters refined using 15 restraints. Despite the relatively high values of the *R*-factors due to the poor quality of the studied crystal, the structural model appears reliable in the light also of results from the Fe-methylphosphonate derivatives (i.e. crystallographic forms (**1**) and (**2**), respectively [9,10]). Fractional coordinates and equivalent atomic displacement parameters are given in Table 2. Selected bond lengths and bond angles are gathered in Table 3.

Table 1
Crystallographic data for $Fe[CH_3(CH_2)_2PO_3)(H_2O)]$ (**1**)

Formula; formula weight [g mol^{-1}]	$C_3H_9O_4PFe$; 195.92
Color	Colorless transparent
Dimensions [mm]	$0.5 \times 0.2 \times 0.02$ bounded by faces {100}, {010}, {001}, respectively
Symmetry	Monoclinic
Space group	$P2_1$ (No. 4)
Z	2
a (Å)	5.7070 (11)
b (Å)	4.8108 (10)
c (Å)	11.818 (2)
β (°)	98.62 (3)
V (Å^3)	320.79 (11)
Density $\rho_{calc.}$ [g cm^{-3}]	2.028
Absorption coeff. μ [mm^{-1}]	2.538
Recording conditions	
Temperature (K)	293
Diffractometer	Kappa CCD-NONIUS
Wavelength λ (Å)	0.71073
θ range for data collection (°)	5.24–27.49
h,k,l ranges	$-7 \leqslant h \leqslant 7$; $-6 \leqslant k \leqslant 6$; $-15 \leqslant l \leqslant 15$
Reflections collected	7014
Absorption corrections	Gaussian method based on the shape of the crystal
Trans. Coeff. Min–Max	0.4726–0.9503
Refinement	
No. of refined parameters	74, using 15 restraints
R indices [1344, $I > 2\sigma(I)$]	$R_{obs} = 0.1349$
R indices [1450, all data]	$R_{all} = 0.1397$
Goodness of fit	$S = 2.113$
Largest peak and hole(e.Å^{-3})	+4.86; −2.02

Table 2
Atomic positions and equivalent isotropic displacement parameters for $Fe[CH_3(CH_2)_2PO_3)(H_2O)]$ (**1**)

Atoms	*x*	*y*	*z*	*U*(eq*, iso)(Å^2)
Fe	0.7446(2)	0.2500(–)	0.9814(1)	0.0174(6)*
P	0.7934(5)	0.8109(7)	0.1425(2)	0.0132(7)*
O(1)	0.788(2)	0.501(2)	0.1284(8)	0.028(2)
O(2)	0.705(2)	0.947(3)	0.8413(9)	0.033(2)
H(1)	0.58(2)	0.83(2)	0.85(1)	0.04(–)
H(2)	0.84(1)	0.85 (3)	0.86(1)	0.04(–)
O(3)	0.017(2)	0.454(2)	0.9161(6)	0.018(2)
O(4)	0.441(2)	0.452 (2)	0.9099(6)	0.016(2)
C(1)	0.852(3)	0.889(3)	0.2896(11)	0.023(3)
H(11)	0.99(1)	0.81(2)	0.333(10)	0.028(–)
H(12)	0.87(2)	1.085(8)	0.28(1)	0.028(–)
C(2)	0.681(3)	0.787(4)	0.364(1)	0.043(4)
H(21)	0.66(3)	0.590(8)	0.35(2)	0.051(–)
H(22)	0.55(2)	0.89(3)	0.32(1)	0.051(–)
C(3)	0.737(4)	0.885(6)	0.489(2)	0.056(6)
H(31)	0.63(2)	0.86(3)	0.544(11)	0.068(–)
H(32)	0.89(1)	0.81(3)	0.52 (1)	0.068(–)
H(33)	0.75(2)	1.081(10)	0.48(2)	0.068(–)

Table 3
Bond lengths (Å) and angles (°) for $Fe[CH_3(CH_2)_2PO_3)(H_2O)]$ (**1**)

	Atoms		Bond 1–2 (Å)	Angle 1–2–3 (°)
1	2	3		
Fe	O1^{ii}		2.10(1)	
	O2^{i}		2.19(1)	
	O3^{v}		2.080(9)	
	O3^{iii}		2.205(9)	
	O4		2.056(9)	
	O4^{iii}		2.287(8)	
P	O1		1.50(1)	
	O3^{iv}		1.533(9)	
	O4^{iv}		1.543(9)	
	C1		1.76(1)	
C1	C2	C3	1.49(2)	114.1(16)
C2	C3		1.55(3)	
C1	H11		0.96(2)	
	H12		0.96(2)	
C2	H21		0.96(2)	
	H22		0.96(2)	
C3	H31		0.96(2)	
	H32		0.96(2)	
	H33		0.96(2)	
O2	H1		0.92(2)	
	H2		0.92(2)	
H1	O2	H2		108(5)
H31	C3	H32		109(5)
H32	C3	H33		110(5)

Symmetry code: (i) $x, -1+y, z$; (ii) $x, y, 1+z$; (iii) $1-x, -0.5+y, 2-z$; (iv) $1-x, 0.5+y, 1-z$; (v) $1+x, y$, z.

2.5.2. Structural characterization of $Fe[(CH_3(CH_2)_{17}PO_3)(H_2O)]$

X-ray powder diffraction pattern of $Fe[(CH_3(CH_2)_{17}PO_3)(H_2O)]$ has been recorded at room temperature and is shown in Fig. 2. The layered nature of the compound is demonstrated by the presence of five well-indexed (0*k*0) reflections in the low-angle region. These reflections were used to estimate the interlayer spacing, which corresponds in this compound to a value of 40.3(1) Å. An attempt to refine this pattern in the orthorhombic space group $Pmn2_1$, which corresponds to the crystal symmetry of the nickel (II) octadecylphosphonate [11], failed.

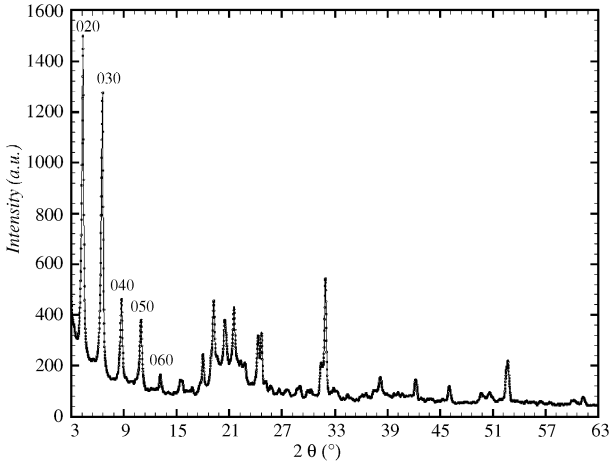

Fig. 2. X-ray powder diffraction patterns of $Fe[CH_3(CH_2)_{17}PO_3)(H_2O)]$ (**2**) showing (0*k*0) reflections.

3. Results

Two new iron (II) alkylphosphonates were prepared from the reaction of the relevant phosphonic acid in water with $FeSO_4 \cdot 7H_2O$ in the presence of urea at temperatures above 80–90 °C under inert atmosphere. Under these conditions, urea decomposes to give ammonium carbonate, thus gradually increasing the pH of the solution to near neutrality. The compounds precipitated as white microcrystalline powders after several days of reflux. This method has been proved to be general for the synthesis and crystal growth of several divalent metal phosphonates. The synthesis was carried out under inert atmosphere in order to avoid the oxidation of Fe(II) into Fe(III). Both the compounds were characterized by elemental analyses, TGA (DSC) and XRPD techniques as well as by the electronic and FT-IR absorption spectroscopy. The TGA of $Fe[(CH_3(CH_2)_2PO_3)(H_2O)]$ (**1**) shows stepwise mass losses. Below 100 °C, <1% of loss is due to adsorbed water. The compound starts to lose coordinated water at 130 °C and it stops at ~180 °C. The observed weight loss at this stage is 8.4%, a value which nearly corresponds to one water molecule per formula unit (the calculated weight loss for one water molecule per formula unit is 9.19%). The compound is then stable up to 470 °C, when it starts to decompose, loosing the organic part of the ligand. In the TGA of $Fe[(CH_3(CH_2)_{17}PO_3)(H_2O)]$ (**2**) the compound starts to lose coordinated water at ~130 °C and it stops at 200 °C. The observed weight loss at this stage is 5.2%, a value that corresponds roughly to one water molecule per formula unit. The calculated weight loss for one water

molecule is 4.40%. Above 280 °C the compound starts to decompose and stops at 540 °C, loosing the 57% of the weight, corresponding to the aliphatic chain of the ligand in the compound.

3.1. Description of the structure of $Fe[(CH_3(CH_2)_2PO_3)(H_2O)]$

The structure of the iron (II) propyl-phosphonate consists of stacking of alternating organic and inorganic layers along the *c* direction as shown in Fig. 3. The iron atom is six-coordinated by oxygen atoms, i.e. five (O1, 2 × O3, and 2 × O4) from the phosphonate groups and one (O2) from the water molecule (where O2–H1 = 0.92(2) Å and O2–H2 = 0.92(2) Å). The [FeO_6] octahedron is slightly distorted with Fe–O distances ranging from 2.056(9) to 2.287(8) Å. Within the inorganic layer, along the *a* direction, adjacent Fe-octahedra are edge-sharing O3–O3 and O4–O4, and the Fe–Fe distances are 3.754(2) and 3.761(2) Å, respectively. The three oxygen atoms, namely O1, O3, and O4 are common to both the Fe-octahedron and the phosphonate group, with P–O distances (Å) of 1.50(1), 1.533(9), and 1.543(9), respectively, in good agreement with P–O distances (1.485, 1.517, and 1.601 Å) found in the Fe-methylphosponate compound. The organic part, i.e. the propyl-group, is connected to the phosphonate group via the P–C1 bonding of 1.76 Å. The C_3H_7-group geometry is in accordance with the expectations, where C–C distances of 1.49(2) Å (C1–C2) and 1.55(3) Å (C2–C3) fit well the tabulated C–C distance (single bond) for an aliphatic chain. In the same way, all the calculated C–H distances in this structure are around 0.96(2) Å. Along the *c* direction, the propyl-groups interpenetrate as in a double-comb. A large vacant site can be observed at each [CH_3–] end of all the propyl-groups. The slabs of neutral $Fe[(C_3H_7PO_3)(H_2O)]$ are then translationally related along the *c*-axis of the unit cell with only van der Waals contacts between them. A quite similar structure was also found for the Fe-methylphosphonate [10].

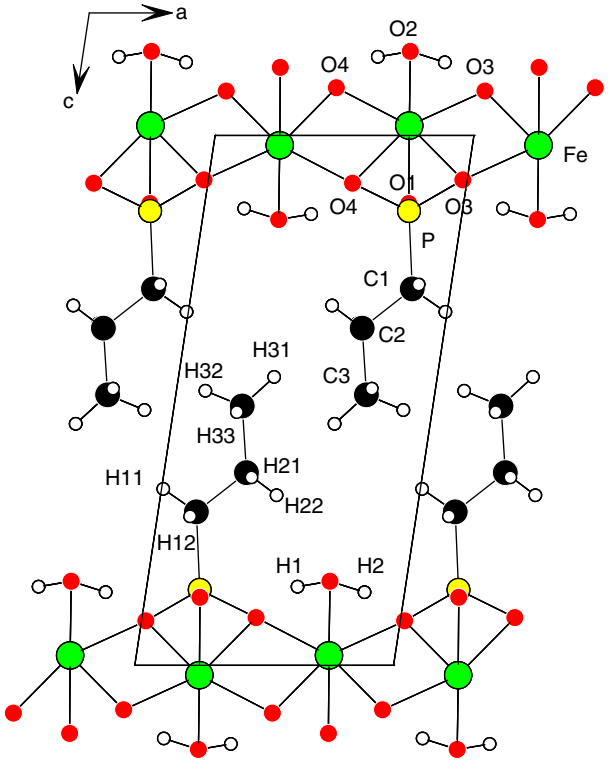

Fig. 3. Unit-cell packing of $Fe[(CH_3(CH_2)_2PO_3)(H_2O)]$ (**1**) viewed along the *b*-axis.

3.2. Structural characterization of $Fe[(CH_3(CH_2)_{17}PO_3)(H_2O)]$

The layered nature of the compound is demonstrated by the analysis of the XRD patterns and of the FT-IR spectrum (see below), and the lattice looks like that of $Ni[(CH_3(CH_2)_{17}PO_3)(H_2O)]$ [17]. The interlayer spacing in the latter, however, is slightly longer, i.e. 42.31 Å instead of 40.3(1) Å found for compound (**2**). The hybrid structure originates from self-assembling of *bi*-layers of Fe(II) octadecylphosphonate.

4. Optical properties

The IR absorption spectrum of $Fe[CH_3(CH_2)_2PO_3)(H_2O)]$ is reported in Fig. 4a. It features two intense bands centred at 3482 and 3438 cm^{-1}, assignable to H–O–H stretching vibration of the coordinated water molecule. The strong and sharp nature of these bands confirms that the water is coordinated to the metal ions in these compounds. The medium band, observed at 1612 cm^{-1}, is assigned to the H_2O bending frequency. Strong bands due to the $[PO_3]^{2-}$ group symmetric (1072 and 994 cm^{-1}) and asymmetric (1046 cm^{-1}) vibrations are observed in the range 1200–970 cm^{-1}. The complete conversion of the phosphonic acid to its Fe(II) salt is demonstrated by the absence of OH stretching vibration of the POH group at ~2700–2550 and 2350–2100 cm^{-1}. Medium peaks are found at 2962, 2941, 2924, 2901 and 2876 cm^{-1} assigned to methyl and methylene groups stretches of the ligand.

The IR absorption spectrum of $Fe[(CH_3(CH_2)_{17}PO_3)(H_2O)]$ (**2**) is reported in Fig. 4b and it shows some remarkable differences when compared with that of the $Fe[(CH_3(CH_2)_2PO_3)(H_2O)]$ (**1**). Intense peaks were found at 2964, 2916, 2848 cm^{-1} together with a shoulder at 2870 cm^{-1} and assigned to the asymmetric methyl [$\nu_a(CH_3)$] and to a symmetric methyl [$\nu_s(CH_3)$] (i.e. 2964 and 2870 cm^{-1}, respectively), to asymmetric methylene [$\nu_a(CH_2)$] and symmetric methylene [$\nu_s(CH_2)$] stretches (i.e. 2916 and 2848 cm^{-1}, respectively) of the octadecyl group. It is well known that the position and the shape of the [$\nu_a(CH_2)$] and [$\nu_s(CH_2)$] absorption bands reflect the conformational order and packing of the aliphatic chains in monolayers [18]. The energy of the [$\nu_a(CH_2)$] band

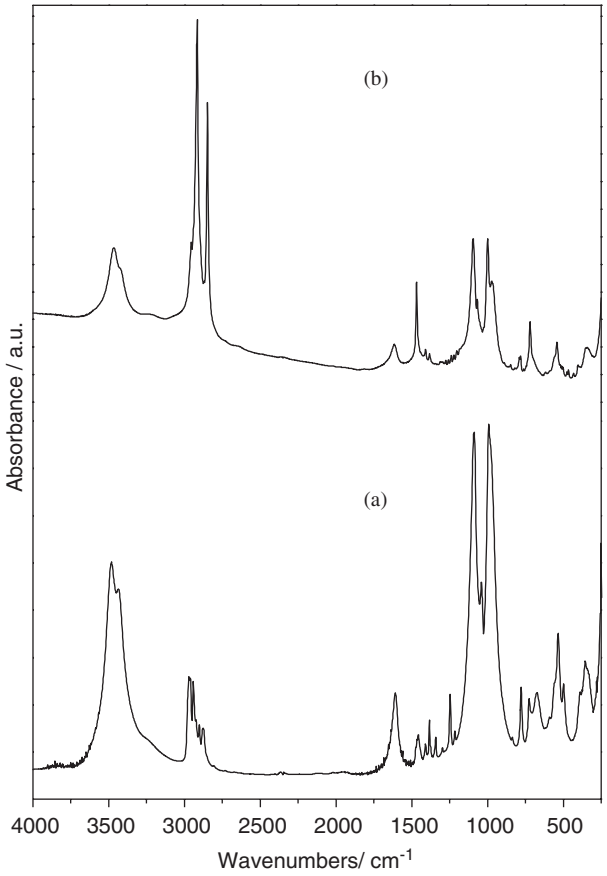

Fig. 4. (a) Absorption FT-IR spectrum of $Fe[(CH_3(CH_2)_2PO_3)(H_2O)]$ (**1**) in the KBr region; (b) absorption FT-IR spectrum of $Fe[CH_3(CH_2)_{17}PO_3)(H_2O)]$ (**2**) in the KBr region.

ranges between 2918 and 2920 cm^{-1} for long-chain hydrocarbons if the aliphatic chain is in *all-trans* conformation. The observed position of the $[\nu_a(CH_2)]$ band at 2918 cm^{-1} implies that alkyl chains are in a fully extended *all-trans* conformation. Another indication of the state of the hydrocarbon chains comes from the $[\nu_s(CH_2]$ band. The peak position of the latter band for crystalline hydrocarbons lies at 2850 cm^{-1} and shifts to a higher value, 2856 cm^{-1}, as the organic chains become less packed. The appearance of the band at 2848 cm^{-1} is consistent with a high-density crystalline phase. The presence of two bands at 3466 and at 3424 cm^{-1} and a band at 1616 cm^{-1} in the spectrum indicates that water is coordinated to the metal ion [19]. In the region 900–1800 cm^{-1} of the infrared spectrum a medium intense peak at 1470 and one weak at 1410 cm^{-1} are assigned to the methylene scissor deformation bands. A progression of weak peaks from 1168 up to 1400 cm^{-1} are assigned to the CH_2 rocking and wagging modes of *all-trans* alkyl chains in this compound (absent in the other one). The band at 1095 cm^{-1} is assigned to the asymmetric $-PO_3$ group stretch, and bands between 1068 and 999 cm^{-1} to the symmetric $-PO_3$ group stretches which split as a result of local symmetry of the phosphonate groups lower than C_{3v}.

5. Magnetic properties

5.1. $Fe[(CH_3(CH_2)_2PO_3)(H_2O)]$ (1)

5.1.1. Dc magnetic susceptibility

Static magnetic susceptibility measurements were made on a polycrystalline sample with an applied magnetic field of 1 kOe in the temperature range 5–300 K by a SQUID magnetometer. The $1/\chi$ vs. T and χT vs. T plots are reported in Fig. 5. The $1/\chi$ vs. T plot is linear above 100 K, showing a typical paramagnetic behaviour. The fit to the experimental data at temperatures above 100 K gave values of Curie, C, and Weiss, θ, constants as 3.81 $cm^3\,K\,mol^{-1}$ and -62 K, respectively. The effective magnetic moment, $\mu_{eff} = 5.52\,\mu_B$, as found from the relation $\mu_{eff} = (8C)^{1/2}$, is within the range observed for high-spin Fe^{2+} ion ($S = 2$ electronic configuration) in octahedral coordination [20]. The negative value of the Weiss constant, $\theta = -62$ K, implies dominant antiferromagnetic nearest-neighbour exchange interactions between the adjacent Fe(II) ions within the distorted square arrays of the inorganic layers. Deviation from Curie–Weiss occurs below $T = 70$ K, where the magnetic susceptibility increase, until a broad peak at ~20 K, is observed. The χT vs. T plot decreases slowly on lowering the temperature down to 25 K and then starts to rise again. Zero-field (zfc) and field-cooled (fc) M vs. T plots under an applied field of 500 Oe have been measured and they are reported in Fig. 6. The two plots do not overlap below $T = 20$ K and the bifurcation point is at T~22 K. The zfc magnetization increases up to ~20 K reaching a broad maximum and then decreases again slowly down to 5 K. The fc magnetization shows a continuous increase on lowering the temperature. Repeating the experiments at an applied magnetic field of 5 kOe, the bifurcation point appears at lower temperature, T~16 K.

5.1.2. Ac magnetic susceptibility

Ac magnetic susceptibilities of a microcrystalline sample of compound (**1**) were recorded as a function of temperature in the temperature region 2–40 K, and at two different frequencies, i.e. 20 and 200 Hz. Fig. 7 shows the real χ' and imaginary χ'' components of ac susceptibility of $Fe[(CH_3(CH_2)_2PO_3)(H_2O)]$. The $\chi' = f(T)$ plot exhibits only a strong peak at $T_N = 22$ K and this is accompanied at the same temperature by a smaller peak in the $\chi'' = f(T)$ curve. The latter reflects important energy losses in the magnetically ordered state and is connected with the domain effects appearing, for instance, in a ferromagnetic or in a weak ferromagnetic state. The temperature at which the peak appears is independent of the frequency, thus definitively indicating the presence of a magnetic ordered state below $T_N = 22$ K.

5.1.3. Isothermal magnetization

Additional insight into the low-temperature magnetic state can be obtained by recording isothermal magnetization

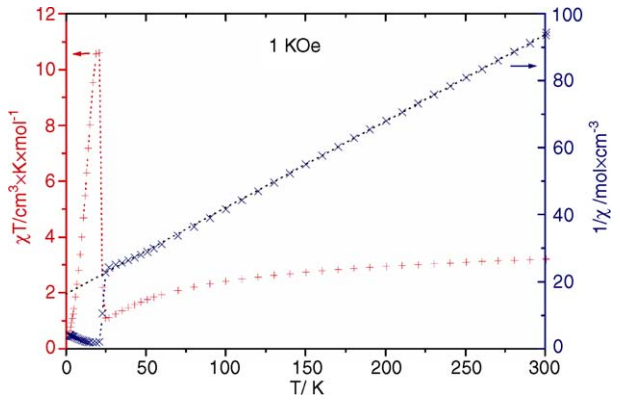

Fig. 5. $1/\chi$ vs. T and χT vs. T plots for Fe[$(CH_3(CH_2)_2PO_3)(H_2O)$] (**1**).

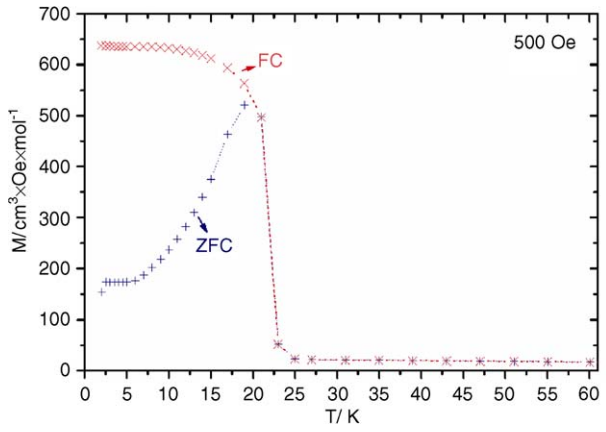

Fig. 6. Dc M vs. T plot for Fe[$(CH_3(CH_2)_2PO_3)(H_2O)$] (**1**) in the temperature range 2–30 K in zero-field, zfc, and field, fc, cooling modes.

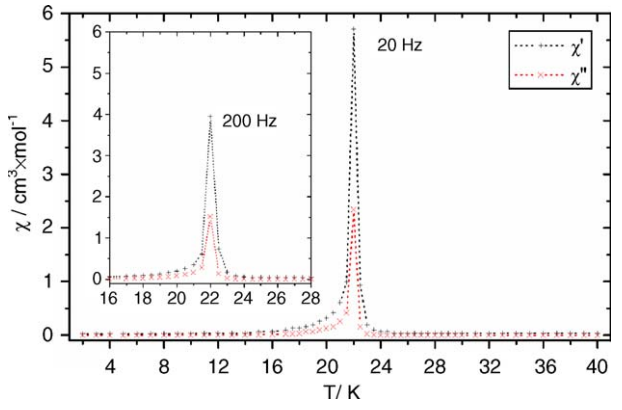

Fig. 7. Temperature dependence of the real (χ') and imaginary part (χ'') of the ac magnetic susceptibility of Fe[$(CH_3(CH_2)_2PO_3)(H_2O)$] (**1**) at two different frequencies of 20 and 200 Hz.

vs. applied magnetic field plots. Hysteresis loops were observed at different temperatures below $T \leqslant 24$ K for applied magnetic fields up to 20 kOe. The plots recorded at $T = 2$ K and that at $T = 19$ K are reported in Fig. 8. From the plot, the values of the saturation magnetization, $M_s(T)$, at the temperature T and that of the coercive field,

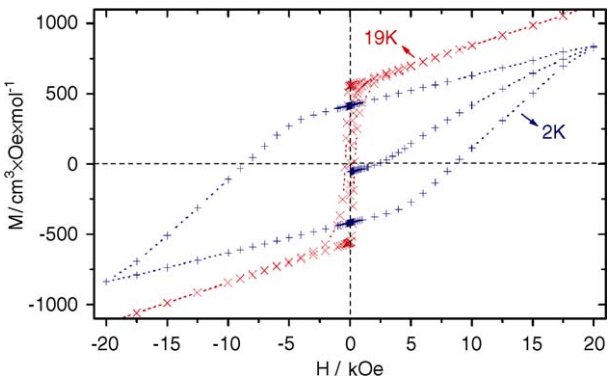

Fig. 8. Hysteresis loops of Fe[$(CH_3(CH_2)_2PO_3)(H_2O)$] (**1**) measured at $T = 2$ and 19 K.

H_c, can be directly obtained. It is possible to estimate the value of M_s from the equation [21]:

$$M(H,T) = M_S(T) + \chi(T)H, \quad (1)$$

where M_s is the saturated weak ferromagnetic moment and χ the antiferromagnetic susceptibility. M_s was determined from the extrapolation to zero field of the linear part of the magnetization curve at high applied magnetic fields and χ was determined as its slope. The value of $M_s(2\,K)$ was found to be 414 $cm^3\,Oe\,mol^{-1}$ and that of the coercive field, H_c, 8630 Oe. It is worth noticing the unusual high value of the coercive field H_c for this kind of materials. The magnetization M_s is ~2% in value of that expected for the fully ferromagnetic aligned moment of Fe^{2+} (i.e. 22.340 $cm^3\,Oe\,mol^{-1}$). This behaviour is typical of a weak ferromagnet. The weakly ferromagnetic state is due to the "spin-canting" [12]. The local spins in this ordered state are not perfectly antiparallel leading to a net spontaneous magnetization which saturates in a small field. Looking at the hysteresis loops recorded at differents temperatures below T_N, a decrease of the coercive field, H_c, is observed on increasing the temperature and this is in relation with the fact that the magnetic anisotropy of Fe^{2+} ions increases as the temperature is lowered. The estimation of the value of M_s (0 K) from the plot is difficult to be made. If we approximate the value of $M_s(0\,K)$ to the M_s found at $T = 2$ K, then the canting angle is estimated to be ~1.1°. At $T = 23$ K, the hysteresis phenomena disappears and the magnetization vs. field plot is not completely linear thus indicating short-range antiferromagnetic interactions. At $T = 24$ K, the isothermal magnetization is linear, as expected for a paramagnet.

5.2. *Fe[$CH_3(CH_2)_{17}PO_3)(H_2O)$] (2)*

5.2.1. *Dc magnetic susceptibility*

Static magnetic susceptibility measurements were performed on a polycrystalline sample of the title compound in the applied magnetic field of 5 kOe in the temperature range of 5–300 K, both in zero and field cooled modes and the zfc molar magnetic susceptibility, χ, plotted as function

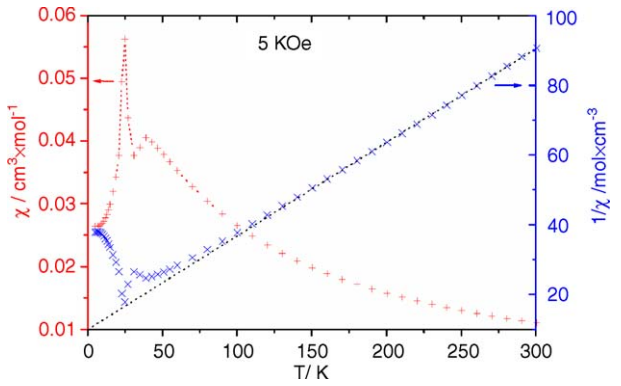

Fig. 9. zfc χ vs. T and $1/\chi$ vs. T plots of Fe[$(CH_3(CH_2)_{17}PO_3)(H_2O)$] (**2**) in the temperature range 5–300 K.

of temperature is reported in Fig. 9. Three different temperature regions can be identified in the plot.

5.2.1.1. High-temperature region. In the first region, i.e. above 100 K, the $1/\chi$ vs. T plot is linear following the Curie–Weiss law. The effective magnetic moment μ_{eff} as deduced from C-value, i.e $3.80\,cm^3\,K\,mol^{-1}$, is in agreement with the expected value for Fe(II) d^6 ($S=2$) high spin electronic configuration (i.e. 5.51 μ_B). The Weiss constant is negative in value, i.e. $\theta=-44$ K, indicating dominant antiferromagnetic interactions between Fe^{2+} ions.

5.2.1.2. Intermediate region. In the second region, i.e. between 30 and 100 K, the χ vs. T plot shows a broad maximum centred at $T\sim39$ K. This broad maximum is typical of a low-dimensional magnet [22]. An analysis of the magnetic behaviour of Fe[$CH_3(CH_2)_{17}PO_3)(H_2O)$] has been carried out in terms of a 2D square-planar Heisenberg model for an $S=2$ system [21]. In the observed model, the position of the maximum in the χ vs. T plot is related directly to the *intra*-planar exchange constant J/k. The relationship between the $T(\chi_{max})$ and the exchange constant coupling value J/k, for an S system, is according to De Jongh and Miedema, given by [22]

$$\tau=\frac{kT(\chi_{max})}{|J|S(S+1)} \quad (2)$$

and

$$\frac{\chi_{max}|J|}{Ng^2\mu_B^2}=0.0547. \quad (3)$$

For an $S=2$ magnetic system, τ is 2.07 and, therefore the estimated J/k value obtained from Eq. (2) is ~-3.1 K, while from Eq. (3) is -2.0 K. This discrepancy indicates no agreement between the experimental data and the suggested model. The reason lies on the fact that the inorganic layers in the lattice are crenelated and that the Fe^{2+} ions, forming a distorted square array by the bridging oxygen atoms of phosphonic ligand, are connected non-equivalently to four nearest neighbours within the slab.

5.2.1.3. Low-temperature region. zfc and fc M vs. T plots have been measured under an applied field of 100 Oe and they are reported in Fig. 10. The two plots do not overlap at temperatures below $T=28$ K. The zfc magnetization increases reaching a maximum at ~26 K and then decreases again down to 15 K. The fc magnetization shows a continuous increase on lowering the temperature and it reaches the value of $\sim120\,cm^3\,Oe\,mol^{-1}$ at $T\sim5$ K. This experiment provides then an indication that the compound is magnetically ordered below $T_N=26$ K.

5.2.2. Ac magnetic susceptibility

Ac magnetic susceptibilities of a sample of compound (**2**) were measured as a function of temperature from 5 to 30 K at three different frequencies, i.e. at 2, 20 and 200 Hz. Fig. 11 shows the real χ' and imaginary χ''components of ac susceptibility of Fe[$(CH_3(CH_2)_{17}PO_3)(H_2O)$]. The $\chi'=f(T)$ plot exhibits a strong peak at $T_N=26$ K, and this is accompanied at the same temperature by a smaller peak in the $\chi''=f(T)$ curve. The latter is connected with the domain effects appearing, for instance, in a ferromagnetic or in a weak ferromagnetic state. The temperature at which the peak appears is independent of the frequency

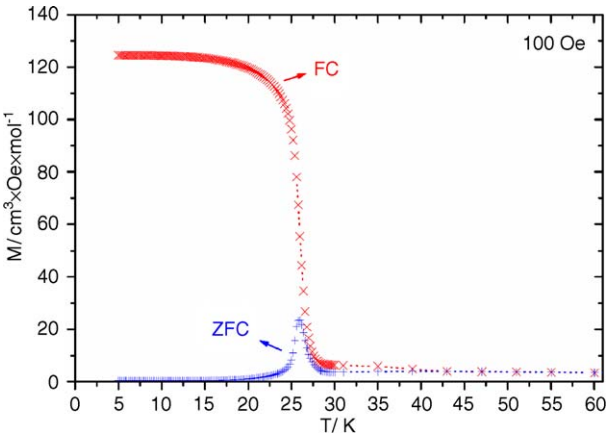

Fig. 10. M vs. T plot for Fe[$(CH_3(CH_2)_{17}PO_3)(H_2O)$] (**2**) in the temperature range 5–40 K in zero-field, zfc, and field, fc, cooling modes.

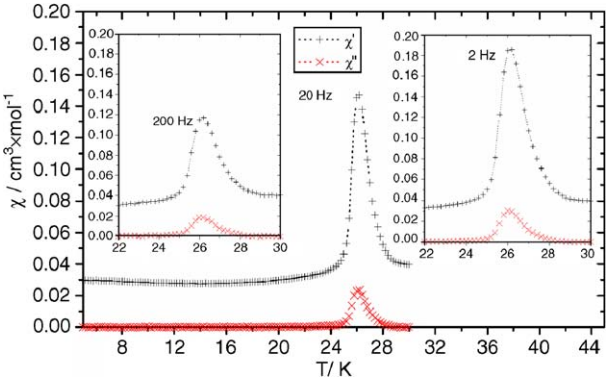

Fig. 11. Temperature dependence of the real (χ') and imaginary part (χ'') of the ac magnetic susceptibility of Fe[$(CH_3(CH_2)_{17}PO_3)(H_2O)$] (**2**) at three different frequencies of 200, 20 and 2 Hz.

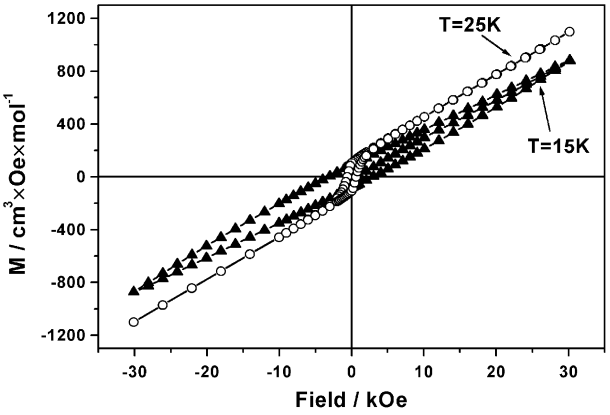

Fig. 12. Hysteresis loop of $Fe[(CH_3(CH_2)_{17}PO_3)(H_2O)]$ (**2**) measured at $T = 15$ and at 25 K.

and so definitively indicating the presence of a magnetic ordered state below $T = 26$ K. No other peaks are observed in the region of 5–30 K.

5.2.3. *Isothermal magnetization*

Isothermal magnetization vs. field plots at different temperatures below T_N were also measured. Two different shapes of them were observed on cooling below T_N. From $T = 26$ to 20 K, the typical sigmoid-shape of a weak ferromagnet with strong anisotropy is observed. Below 15 K, the hysteresis loop takes a shape of an ellipsoid (see Fig. 12). The latter type of shape has been observed previously in Langmuir–Blodgett Mn(II) octadecylphosphonate films, when the applied field is oriented perpendicular to the plane of the film [23,24]. The hysteresis loop at $T = 25$ K shows that the value of magnetization increases non-linearly up to 150 $cm^3\,Oe\,mol^{-1}$ and then linearly up to 30 kOe (i.e. the highest applied magnetic field) according to Eq. (1). From the plot taken at $T = 25$ K, the values of the saturation magnetization, M_s, and of the coercive field, H_c, could be directly obtained and they are 155 $cm^3\,Oe\,mol^{-1}$ and 600 Oe, respectively.

6. Discussion

Two new layered iron (II) alkylphosphonates, $Fe[(C_nH_{2n+1}PO_3)(H_2O)]$ $n = 3,18$, have been prepared and characterized. They differ only in the number of carbon atoms present in the aliphatic chain of the ligand. The crystal and molecular structure of a white platelet crystal of compound (**1**) was solved by X-ray single crystal studies. It crystallizes in the non-centrosymmetric monoclinic space group $P2_1$ with a typical hybrid layered structure of the inorganic and organic layers alternating along the *c*-axis of the unit-cell, with an interlayer of 11.82 Å. The inorganic sheet is made of octahedrally coordinated Fe(II) ions, and the octahedron is distorted, due to the fact that two oxygens of the phosphonate ligand bond to two Fe atoms and one acts a monodentate. The structure of the inorganic layers is similar to the other reported iron (II) alkylphosphonates. A layered hybrid structure is also shown by $Fe[(CH_3(CH_2)_{17}PO_3)(H_2O)]$, but the inorganic layers are separated apart and the interlayer spacing is 40.3 Å.The full structure of the latter has not been solved, but an additional structural information on the layout of the organic groups within the lattice has been provided by the infrared spectroscopy studies [18], which indicate that alkyl chains are in a fully extended *all-trans* conformation. On the basis of these data we can confirm that the lattice of compound (**2**) is then similar to that found in $Ni[(CH_3(CH_2)_{17}PO_3)(H_2O)]$ [17].

The reported compounds are both weak ferromagnets at low temperatures. They order at two slightly different critical temperatures, i.e. at $T_N = 22$ K for compound (**1**), and at $T_N = 26$ K for compound (**2**). The values of the critical temperatures T_N along the series of the known iron (II) phosphonates (see Table 4) range between $T = 22$ and 26 K and are independent of the interlayer spacings. The lowest T_N values have been observed in the iron (II) phenyl- and iron (II) propylphosphonates, where the interlayer spacings are in between those of the first and the last member of the series. The fact that iron (II) octadecylphosphonate shows the same value of T_N of the first member of the series, i.e. $(NH_4)FePO_4$ [25], means a similar temperature dependence of the in-plane correlation length [26]. The small difference observed in the values of T_N along the series is difficult to rationalize. It might depend in the first approximation on the value of the exchange constant, J/k, which is a function of the superexchange pathways allowed in these structures. The $|T_N/\theta|$ ratio along the series is in average of ~0.5 (see Table 4) and this experimental finding is consistent with the two-dimensional nature of the magnetic exchange; the molecular field in fact predicts $|T_N/\theta|$ ratio of ~1. Indeed, iron (II) octadecylphosphonate at low temperatures shows a broad maximum in the χ vs. T plot at T_{max}~39 K, which is typical of a low-dimensional magnetic system, and this is in agreement with the observed layered structure. Below T_N a weak ferromagnetic state is present and is due to the "spin-canting" [12]. The local spins in this ordered state are not perfectly antiparallel, leading to a net spontaneous magnetization which saturates in a small field. Two mechanisms have been suggested for producing spin canting: (1) single-ion magnetic anisotropy [27,28] and (2) the so-called antisymmetric Dzyaloshinsky–Moriya (D–M) exchange coupling [29], which may occur between neighbouring centres and compete with isotropic Heisenberg antiferromagnetic exchange. The first mechanism operates when there are two equivalent sites of magnetic ions, but the directions of their anisotropy axes are different, as in NiF_2. D–M mechanism acts to cant the spins, because the coupling energy is minimized when the two spins are perpendicular to each other. This coupling operates in addition to isotropic Heisenberg exchange and depends on the symmetry of the crystal, (i.e. the interacting magnetic ions in the unit-cell cannot be related by an inversion centre of symmetry). Now, in $Fe[(RPO_3)(H_2O)]$, the symmetry of

Table 4
Magnetic parameters of Fe(II) phosphonates

Compound	T_N (K)	θ (K)	T_N/θ	Spacegroup	a (Å)	b (Å)	c (Å)	β (°)	Interlayer spacing (Å)	Ref.
$(NH_4)FePO_4$	26.0	−65	0.40	$Pmn2_1$	5.666(1)	8.821(2)	4.831(1)		8.82	[25]
$Fe[(CH_3PO_3)(H_2O)]$ form (**1**)	25.0	−59	0.42	$Pna2_1$	17.538(2)	4.814(1)	5.719(1)		8.77	[9]
$Fe[(CH_3PO_3)(H_2O)]$ form (**2**)	25.0	−59	0.42	$Pmn2_1$	5.718(1)	8.809(1)	4.815(1)		8.81	[10]
$Fe[C_2H_5PO_3)(H_2O)]$	24.5	−43	0.57	$P1n1$	5.744(3)	10.33(1)	4.856(8)	91.0	10.33	[6]
$Fe[(C_3H_7PO_3)(H_2O)]$	22.0	−62	0.35	$P2_1$	5.707(1)	4.811(1)	11.818(2)	98.6(3)	11.65	[a]
$Fe[(C_6H_5PO_3)(H_2O)]$	21.5	−56	0.38	$Pmn2_1$	5.669(8)	14.453(2)	4.839(7)		14.45	[7]
$Fe_2[(O_3P(CH_2)_2PO_3)(2H_2O)]$	25.0	−52	0.48		5.67(1)	15.23(3)	4.82(1)		15.23	[8]
$Fe[(C_{18}H_{37}PO_3)(H_2O)]$	26.0	−44	0.59			40.3(1)			40.3	[a]

[a] This work.

the space groups are low enough to allow the Dzyaloshinsky–Moriya (D–M) exchange coupling to operate, this because the adjacent metal ions in the square are bridged by a non-centrosymmetric ligand. The antisymmetric exchange is then the origin for the canting of the spins and the magnitude of the spontaneous magnetization depends on the canting angle. The D–M mechanism has been referred to explain weak ferromagnetism in manganese (II) alkylphosphonates [30]. Moreover, Fe(II) ion in octahedral field has a ground state $^5T_{2g}$, and the low site symmetry present in the title compounds generates the anisotropy in the g-value. The role of single-ion anisotropy is confirmed also from the unusual high values of the coercive fields H_c at low temperatures observed in the iron (II) alkylphosphonate [25]. Iron (II) alkylphosphonates represent the second family of layered metal(II) phosphonates which show weak ferromagnetism, being manganese(II) alkylphosphonate series the first one [30]. There is ~10 K of difference in the absolute values of critical temperatures between the two series of compounds, being those of the iron derivatives higher in value. Although the structures are basically the same, there exist certain differences. The first is represented by the decrease of volume of the unit-cell as a function of ionic radius ($r_{Mn} > r_{Fe}$). A comparison of the volumes of the corresponding unit-cell of the isomorphous and isostructural $Mn[(CH_3PO_3)(H_2O)]$ [30] and $Fe[(CH_3PO_3)(H_2O)]$ [10] shows in fact that the manganese compound has a bigger volume (i.e., 251.27 against 242.55 Å^3 for iron compound). This means that all the structural parameters, such as M–O bond distances, change accordingly. Now, according to the molecular field theory of antiferromagnetism [12] the value of the critical temperature is proportional to the magnetic exchange J/k through the relation:

$$T_N = \left(\frac{2}{3}\right) z\,[S(S+1)]\,J/k. \quad (4)$$

By assuming the same value of z, (i.e. $z = 4$), for the two metal phosphonates, and by substituting in the above-mentioned relation $S = 2$ (Fe^{2+}) and $S = 5/2$ (Mn^{2+}) and the two corresponding experimental values of T_N, it immediately appears that exchange constant J/k for the iron compound must be higher than that of the manganese one. The lower value of the unit-cell volume implies then shorter metal–oxygen bonds in the iron (II) compound. This also implies a stronger nearest-neighbour exchange coupling between the oxygen bridged iron atoms arranged in a distorted square array within the inorganic layers.

In summary, this paper describes the syntheses and crystal structure of two new iron (II) alkylphosphonates. They exhibit a two-dimensional hybrid organic-inorganic structure. The magnetic properties of both compounds (**1**) and (**2**) show dominant antiferromagnetic interactions between magnetic centres. Below $T = 22$ and 26 K, they are weak ferromagnets.

Acknowledgments

This work is supported by the Consiglio Nazionale delle Ricerche (Italy) and the CNRS in the framework of their bilateral collaboration agreement. The Italian Ministero of Education (MIUR) is also acknowledged for financial support (FIRB programme).

Supporting Information Available: CIF of $Fe[CH_3(CH_2)_2PO_3)(H_2O)]$. This material is available free of charge on Internet.

References

[1] P. Gomez-Romero, C. Sanchez (Eds.), Functional Hybrid Materials, Wiley-VCH, Weinheim, 2004.
[2] [a] G. Alberti, in: J.-M. Lehn (Ed.), Comprehensive Supramolecular Chemistry, vol. 7, Pergamon Press, Oxford, 1996, pp. 151–185.; [b] A. Clearfield, Progr. Inorg. Chem. 47 (1998) 371–510.
[3] [a] G. Cao, H. Hong, T.E. Mallouck, Acc. Chem. Res. 25 (1992) 420–427; [b] G. Cao, H. Lee, V.M. Lynch, L.M. Yacullo, Chem. Mater. 5 (1993) 1000–1006.
[4] C. Bellitto, in: J.S. Miller, M. Drillon (Eds.), Magnetism: Molecules to Materials, vol. 2, Wiley-VCH, Weinheim, 2001, pp. 425–456.
[5] [a] C. Bellitto, F. Federici, S.A Ibrahim, J. Chem. Soc. Chem. Commun. (1996) 759–760; [b] C. Bellitto, F. Federici, S.A. Ibrahim, Chem. Mater. 10 (1998) 1076–1082.
[6] [a] B. Bujoli, O. Pena, P. Palvadeau, J. LeBideau, C. Payen, J. Rouxel, Chem. Mater. 5 (1993) 583–587;

[b] P. Palvadeau, J. LeBideau, C. Payen, J. Rouxel, J. Magn. Magn. Mater. 140 (1995) 1719–1720.
[7] A. Altomare, C. Bellitto, S.A. Ibrahim, M.R. Mahmoud, R.R. Rizzi, J. Chem. Soc. Dalton (2000) 3913–3919.
[8] [a] C. Bellitto, F. Federici, S.A. Ibrahim, M.R. Mahmoud, MRS Fall Meetings Proc. 547 (1999) 487–492;
[b] C. Bellitto, F. Federici, A. Altomare, R.R. Rizzi, S.A. Ibrahim, Inorg. Chem. 39 (2000) 1803–1808.
[9] C. Bellitto, F. Federici, M. Colapietro, G. Portalone, D. Caschera, Inorg. Chem. 41 (2002) 709–714.
[10] P. Léone, P. Palvadeau, K. Boubekeur, A. Meerschaut, C. Bellitto, E.M. Bauer, G. Righini, P. Fabritchnyi, J. Solid State Chem. 178 (2005) 1125–1132.
[11] C. Bellitto, E.M. Bauer, S.A. Ibrahim, M.R. Mahmoud, G. Righini, Chem. Eur. J. 9 (2003) 1324–1331.
[12] R.L. Carlin, Magnetochemistry, Springer, Berlin, 1986, pp. 149–152.
[13] C. Bellitto, E.M. Bauer, M. Colapietro, G. Portalone, G. Righini, Inorg. Chem. 42 (2003) 6345–6351.
[14] R.F. Hudson, Structure and Mechanism of Organophosphorus Chemistry, Academic Press, New York, 1965.
[15] XPREP, Data preparation & Reciprocal Space Exploration, Ver. 6.14 UNIX, Copyright ©, Brucker Nonius, 2003.
[16] G.M. Sheldrick, SHELXTL, Ver. 6.12 UNIX, Copyright ©, Brucker-AXS, 2001.
[17] M.D. Porter, T.B. Bright, D.L. Allara, C.E.D. Chidsey, J. Amer. Chem. Soc. 109 (1987) 3559–3568.
[18] K. Nakamoto, Infrared and Raman Spectra of Inorganic and Coordination Compounds, third ed, Wiley, New York, 1978.
[19] B.N. Figgis, Introduction to Ligand Fields, Interscience, London, 1966, pp. 220–222.
[20] P. Palacio, in: E. Coronado, P. Delhaes, D. Gatteschi, J.S. Miller (Eds.), Molecular Magnetism from Molecular Assemblies to the Devices, NATO-ASI, Series E.321, p. 57.
[21] [a] M.E. Lines, J. Phys. Chem. Solids 31 (1970) 101–116;
[b] G.S. Rushbrooke, P.J. Wood, Mol. Phys. 1 (1958) 257–285.
[22] J. DeJongh, A.R. Miedema, Adv. Phys. 23 (1) (1974) 64.
[23] C.T. Seip, G.E. Granroth, M.W. Meisel, D.R. Talham, J. Amer. Chem. Soc. 119 (1997) 7084–7094.
[24] G.E. Fanucci, J. Krzysted, M.W. Meisel, L.C. Brunel, D.H. Talham, J. Amer. Chem. Soc. 120 (1998) 5469–5479.
[25] J.E. Greedan, K. Reubeunbauer, T. Birchall, M. Ehlert, J. Solid State Chem. 77 (1988) 376–388.
[26] M. Drillon, P. Panissod, J. Magn. Magn. Mater. 188 (1998) 93–99.
[27] T. Moriya, Phys. Rev. 120 (1960) 91–98.
[28] T. Moriya, Phys. Rev. 117 (1960) 635–647.
[29] I. Dzyaloshinsky, J. Phys. Chem. Solids 4 (1958) 241–255.
[30] S.G. Carling, P. Day, D. Visser, R.K. Kremer, J. Solid State Chem. 106 (1993) 111–119.